

Katrin Suder · Klaus Funke · Yongqiang Zhao  
Nicolas Kerscher · Thomas Wennekers  
Florentin Wörgötter

## Spatial dynamics of receptive fields in cat primary visual cortex related to the temporal structure of thalamocortical feedforward activity

### Experiments and models

Received: 21 June 2001 / Accepted: 6 February 2002 / Published online: 13 April 2002  
© Springer-Verlag 2002

**Abstract** We investigated how changes in the temporal firing rate of thalamocortical activity affect the spatio-temporal structure of receptive field (RF) subunits in cat primary visual cortex. Spike activity of 67 neurons (48 simple, 19 complex cells) was extracellularly recorded from area 17/18 of anesthetized and paralyzed cats. A total of 107 subfields (on/off) were mapped by applying a reverse correlation technique to the activity elicited by bright and dark rectangles flashed for 300 ms in a 20×10 grid. We found that the width of the (suprathreshold) discharge fields shrank on average by 22% during this 300-ms-long stimulus presentation time. Fifty-eight subfields (54%) shrank by more than 20% of peak width and only ten (less than 10%) showed a slight increase over time. The main size reduction took place 40–60 ms after response onset, which corresponded to the transition from transient peak firing to tonic visual activity in thalamocortical relay cells (TC). The experimentally obtained RFs were then fitted with the aid of a neural field model of the primary visual pathway. Assuming a Gaussian-shaped spatial sensitivity profile across the RF subfield width, the model allowed us to estimate the sub-threshold RF (depolarization field, D-field) from the minimal discharge field (MDF). The model allowed us to test to what degree the temporal dynamics of thalamocortical activity contributes to the spatiotemporal changes of cortical RFs. To this end, we performed the fitting procedure either with a pure feedforward model or with a field model that also included intracortical feedback.

Spatial and temporal parameters obtained from fits of the experimental RFs matched closely to those achieved by simulating a pure feedforward system with the field model but were not compatible with additional intracortical feedback. Thus, our results show that dot stimulation, which optimally excites thalamocortical cells, leads to a shrinkage with respect to the size of the RF subfield at the first transient response of visual cortical RFs which seems mainly due to a change in the thalamic firing pattern. In these experiments little or no influence from intracortical sources was observed, which, however, may play a role when using more complex visual stimuli.

**Keywords** Thalamocortical response dynamics · Cortical spatiotemporal receptive field dynamics · Field model · Depolarization field · Discharge field · Cat

### Introduction

Numerous recent studies have shown that the receptive fields (RFs) of neurons in the primary visual cortex of mammals are not static over time and space but show spatiotemporal dynamics at different time scales. Slowly developing and usually long lasting changes occur during so-called plastic changes (cortical plasticity), which are related to circuit reorganizations after lesions (Gilbert 1996; Eysel and Schweigart 1999) and use-dependent synaptic plasticity (Eysel et al. 1998). Much faster changes in size, sensitivity, and signs of RF components can be observed even during the time course of a single visual response (DeAngelis et al. 1993) and are thought to be related to changes in synaptic efficiency, adaptive processes intrinsic to the neuron, and the concerted action of feedforward and feedback circuits. These fast dynamics of RF parameters seem to contribute to, or may even generate, higher-order RF properties such as selectivity for the direction of a moving contrast border (DeValois and Cottaris 1998; Murthy and Humphrey 1999) or context-dependent

K. Suder · K. Funke (✉) · Y. Zhao · N. Kerscher  
Institute of Physiology, Department of Neurophysiology,  
Ruhr University, 44780 Bochum, Germany  
e-mail: funke@neurop.ruhr-uni-bochum.de  
Tel.: +49-234-3223944, Fax: +49-234-7094192

T. Wennekers  
Max Planck Institute for Mathematics in the Sciences,  
Inselstrasse 22–26, 04103 Leipzig, Germany

K. Suder · F. Wörgötter  
Department of Psychology, University Stirling, Stirling FK8 4LA,  
Scotland

modification of the center response by regions surrounding the classic RF (Knierim and van Essen 1992; for a review, see Wörgötter and Eysel 2000). While the latter is mainly related to lateral cortical interactions, direction-selectivity may evolve from thalamocortical inputs with different visual delays.

Commonly, the RF is defined as the retinal area where a sensory neuron responds to stimulation (Levine and Shefner 1991). The area where a neuron responds with action potentials is called the (*output*) *discharge* field (Hartline 1940), whereas the usually larger area of synaptically evoked (subthreshold) membrane potential changes is called the *synaptic (integration)* field (Kuffler 1953). Since our analysis is only concerned with excitatory inputs, we will use the terms D-field for subthreshold depolarization and minimal discharge field (MDF) for the suprathreshold responses (see Bringuier et al. 1999 for an investigation of the relation between synaptic field and MDF).

Recently, we have demonstrated that even a very “simple” stimulus such as a flashing dot or bar can evoke dynamic cortical responses reflected by spatiotemporal changes of RF sensitivity nature (Wörgötter et al. 1998). In response to the flashing stimulus (300 ms duration), the “early” RF was wider than the “late” RF. The current study was undertaken to analyze whether the shrinkage of the cortical RF subfields during visual stimulation with a spot may be related to the temporal pattern of the thalamic input, which changes from a transient overshoot of activity (peak) to a tonically elevated firing while the stimulus is still present. Alternatively, intracortical feedback may contribute to the shrinkage of the RF. This, however, may be less likely given the structure of the stimulus (flashing dot), which does not drive cortical cells very strongly. To test this hypothesis, we designed a field model of the primary visual pathway which allows quantifying of relevant parameters and fitting of the experimentally obtained RFs. Assuming a Gaussian-shaped efficiency profile of thalamic inputs across the dendritic tree of a cortical neuron (McLean and Palmer 1994; Reid and Alonso 1995; Bringuier et al. 1999), the model also allows us to determine the extent of the D-field of the neuron from the suprathreshold field, the MDF (Bringuier et al. 1999). The field model was used in two ways: First, we determined how the shape of cortical RFs depends on the input structure, which was either a pure thalamocortical input, with realistic temporal dynamics of firing, or intracortical feedback in addition to pure thalamocortical input. Secondly, we used the field model to fit 107 subfields (on or off) of cortical RFs to obtain the width of the subthreshold D-field together with several other descriptive spatial and temporal parameters. Finally, we compared the results of the RF fits with the model simulations and found that the results of the pure thalamocortical feedforward model much better explain the experimentally obtained spatiotemporal RF parameters than the feedback model (Wörgötter et al. 1998).

Parts of this study have been published as an Abstract.

## Materials and methods

### General procedures

Data were obtained from single-unit recordings in the primary visual pathway (dorsal lateral geniculate nucleus, dLGN; perigeniculate nucleus, PGN; and areas 17 and 18) of six cats under constant mesopic luminance. Surgery enabling infusion and artificial respiration were performed under initial ketamine hydrochloride-xylazine anesthesia (Ketanest 20–25 mg/kg; Parke-Davies, Germany; Rompun 1–2 mg/kg; Bayer, Germany). Trepanations were made to allow vertical access to the dLGN, PGN, and areas 17 and 18 for single-unit recordings and for epidural electroencephalography (EEG) registration with silver ball electrodes. While still under Ketanest-Rompun anesthesia, cats were paralyzed by alcuronium chloride infusion ( $0.15 \text{ mg kg}^{-1} \text{ h}^{-1}$ ) dissolved in 15% glucose-Ringer solution, Alloferin 10; Hoffmann-La Roche, Germany) through a cannula in the femoral artery, directly followed by artificial ventilation with  $\text{N}_2\text{O}$  and  $\text{O}_2$  (70:30). Sufficient analgesia was achieved by adding 0.6–2.5% halothane. The level of anesthesia was enhanced (halothane 1.5–2.5%) during any potentially noxious procedure (changing contact lenses, penetration of the dura) and when increases in blood pressure or heart rate might signal that the animal was in distress. During recording sessions, which started a couple of hours after surgery and lasted for up to 9 days, the anesthetic level was reduced to 0.6–1.5% halothane to avoid intoxication of the liver and to allow for sufficiently long recording periods under physiological conditions. All wound margins and pressure points were treated with the local anesthetic xylocaine (2%; Astra Chemicals, Germany). To maintain the physiological state of the animal, the end-expiratory  $\text{CO}_2$  was kept almost constant at approximately 3.8%, the body temperature was held at  $38.5^\circ$ , and infections were prevented by application of broad-band antibiotics (0.5 ml Chassoton i.m.; Chassot, Germany; and drops of Isoptomax topically applied to the cornea; Alcon Pharma, Germany). Mydriasis and retraction of the nictitating membranes was achieved by topical administration of atropine sulfate (1% Atropin-Pos; Ursapharm, Germany) and phenylephrine hydrochloride (5% Neosynephrin-Pos; Ursapharm, Germany). The corneas were protected against dehydration with zero-power contact lenses, and the optics were corrected for a viewing distance of 57 cm with spectacle lenses of 5–7 diopters. The animal was finally killed under maximal anesthesia (4% halothane) by exchanging the blood with Ringer solution, followed by perfusion with 4% paraformaldehyde to enable histological studies of the brain. All experimental procedures conformed to the guidelines of the German animal welfare laws and were approved by the local animal welfare committee.

### Recordings and stimulation

Single-unit recordings were performed with glass micropipettes of 3–7  $\mu\text{m}$  outer-tip diameter, filled with 3 M NaCl solution. Following conventional electronic amplification, single-unit action potentials were separated from noise using a window discriminator with nonlinear gain of amplification (Osaka et al. 1988) and threshold detection. Spike occurrence times were digitally stored on the hard disk of a PC by the aid of a laboratory interface (model 1401; Cambridge Electronic Design, UK). Cortical simple and complex cells of area 17 were distinguished by standard methods (Skottun et al. 1991). Position and best orientation of RFs were determined by manually projecting a bright bar on a plotting screen. For the RF mapping procedure, small bright and dark dots of  $0.5 \times 0.5$  to  $1.0 \times 1.0^\circ$  or small bars of  $0.5 \times 1.0$  to  $1 \times 2^\circ$  (adapted to the size of the RF) and of 50% contrast to background ( $2 \text{ cd/m}^2$ ) were presented on an oscilloscope screen (Tektronics 608; frame rate 200 Hz) in a quasi-random order. Depending on eccentricity and cell type, a stimulus size was chosen which was less than 30% of the width of the receptive subfield during the late response. Spatiotemporal control of stimuli was achieved with the cathode ray image generator Picasso (Innisfree; Cambridge, Mass., USA) un-

der computer control. Single bright or dark dots were presented about 200 times at every location within a  $20 \times 10$  grid of  $10 \times 5^\circ$  for cortex cells and  $10 \times 10$  grid of  $5 \times 5^\circ$  for the smaller RFs of dLGN cells. The grid was always centered on the RF. In the case of cortical recordings, its orientation was adapted to the orientation of the RF. The long axis of the grid ( $10^\circ$ ) was perpendicular to the preferred orientation of the RF in order to achieve sufficient mapping of neighboring RF subfields and because our previous studies indicated stronger changes in RF subfield width than length (Wörgötter et al. 1998). Each dot was presented for 300 ms to elicit not only initial phasic but also subsequent tonic visual responses. Accordingly the total recording time for a single cell often exceeded 4 h. The fine grid resolution and the necessarily long measuring time make an anesthetized and relaxed preparation indispensable, because absolutely reliable eye-positioning is necessary.

Reverse-correlation technique (DeAngelis et al. 1993; Eckhorn et al. 1993; Jones and Palmer 1987) or a forward correlation technique equivalent to peristimulus time-histogram calculation was used to create spatial ( $x, y$ ) RF maps separately for bright and dark dot stimulation. To this end, spikes occurring within a certain time window after stimulus onset were counted for each grid position. In addition, RF time plots ( $x, t$ ) were calculated to demonstrate the spatiotemporal dynamics of the RF. To this end, spikes were counted in short, progressing time windows of 10 ms, starting with stimulus onset. To demonstrate variations only in the  $x$ -dimension of the RF, all pixels along the  $y$ -axis corresponding to the long axis of the RF were summed up. To determine the width of a subfield, we used the half-width at half-height measured across the resulting peak. The polarity of a subfield is determined by its responsiveness to bright (on-subfield) or dark (off-subfield) stimuli.

## Results

### Spatiotemporal changes of experimental RFs

In this section we will describe the basic experimental finding, the shrinkage of cortical RF components, partly published by Wörgötter et al. (1998). Quantification of this phenomenon is based on 107 subfields (on and off) of 67 cortical cells (48 simple, 19 complex) at an eccentricity of  $3\text{--}10^\circ$ . If clearly delineated in the maps, one on- and one off-field of a cell was included in the analysis. For comparison, we also analyzed the RFs of 53 relay cells of the dLGN. Generally, dLGN recordings were performed simultaneously with the cortical recordings in the same cat using two separate electrodes. We thereby tried to enable a topographical match of RFs in dLGN and cortex to achieve comparable ranges of eccentricity for the two populations and similar EEG states. The match, however, was not sufficient to find coupled cells by cross-correlation analysis. The spectral composition of the EEG was used to sort the spike data into samples obtained during synchronized (strong delta-band) and less-synchronized EEG (weak delta-band).

A thalamic response – evoked by a sudden change in contrast – starts with a strong initial, phasic response (see Fig. 1A). This initial response is followed by tonically elevated activity during continuing stimulation (which has a large amplitude during nonsynchronized EEG, while it is less strong or even absent during synchronized EEG). In our experiments we used a stimulus duration of 300 ms to map RFs. This time is long enough to enable the transition of thalamic visual activity from

the initial phasic to the following tonic activity, a process which seems to be fundamental to spatiotemporal dynamics of cortical responses. In the present study, we considered only those episodes for analysis which were recorded during a less synchronized state that allows for tonic visual activity to develop in the dLGN. Much shorter (less than 50 ms) stimuli were used in other studies when measuring discharge fields with flashing dots (reverse correlation technique; DeAngelis et al. 1993; Eckhorn et al. 1993). These short stimuli will only evoke phasic responses in subcortical units. In the next section, we will show detailed results from cortical cells, then we will briefly explain our findings in the dLGN.

### Cortical RF restructuring

To demonstrate changes of the spatial characteristics of cortical MDFs, the width orthogonal to the long axis of the field was plotted as a function of time after stimulus onset with time windows of 10 ms duration (Fig. 1C–G). It can be seen that the change from phasic to tonic response in thalamic cells (Fig. 1A) corresponds to a restructuring from wide to narrow cortical MDFs, occurring during the response: The first transient cortical response (50–90 ms), which is related to the transient dLGN response, corresponds to a wide MDF, which shrinks during the tonic response.

The statistical analysis of the observed shrinkage effect is shown in Fig. 2. The histogram quantifies the temporal changes of cortical MDFs. The size of the dominant (on or off) subfield was compared at 70 ms with that at 200 ms after stimulus onset for 107 subfields. Figure 2 shows the number of subfields grouped as a function of the change in subfield size. The resulting distribution exhibits a mean subfield shrinkage of  $22.8 \pm 12.9\%$  (median 23.1%). Of 107 subfields, 58 shrank by more than 20% only less than 10% showed an increase in size with progressing time.

### RF restructuring in the dLGN

This study is mainly concerned with the rather prominent effect of RF shrinkage in the cortex, but we also observed a similar but much less pronounced effect in the dLGN. Usually, the RFs of thalamic relay cells, recorded simultaneously with cortical cells of corresponding topography ( $n=53$ ), were first mapped with an array of stimuli optimized for cortical RFs ( $20 \times 10$  grid of  $10 \times 5^\circ$ , bars of  $0.5 \times 1$  to  $1 \times 2^\circ$ ). According to the smaller thalamic RFs, these maps allowed only a gross estimation of spatiotemporal changes and indicated only marginal changes. Therefore, 17 dLGN relay cells were additionally mapped with smaller stimuli ( $0.5 \times 0.5^\circ$ ) in a grid of  $10 \times 10$  positions covering an area of  $5 \times 5^\circ$ . This sample showed a similar *relative* shrinkage of RFs (on average,  $17.9\% \pm 29\%$ , median 20.3%); however, the absolute changes are far smaller (on average,  $0.2^\circ$ ) than those

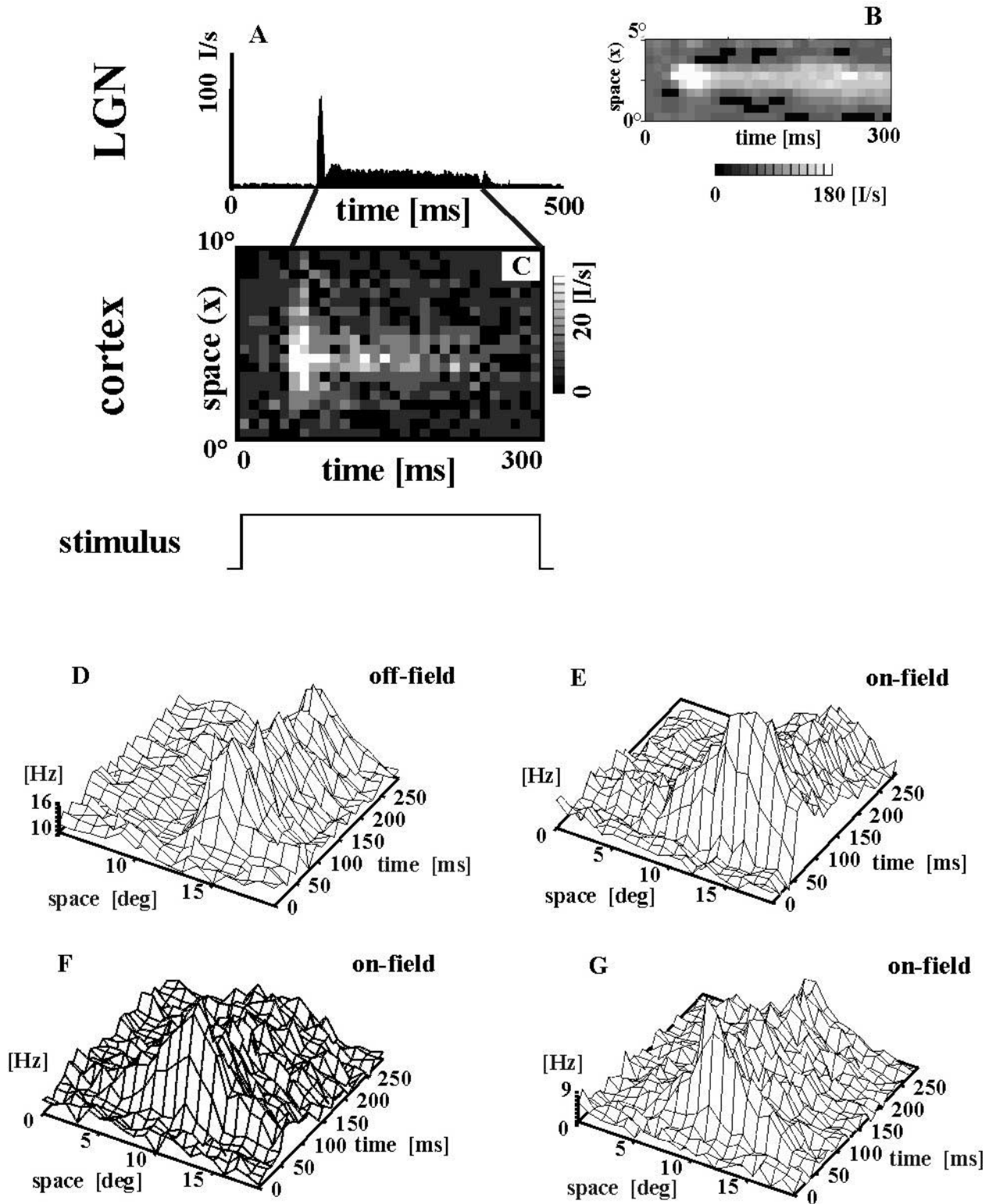


**Fig. 1** A Peristimulus-time histogram of a dorsal lateral geniculate (*LGN*) cell responding to a light stimulus recorded during nonsynchronized electroencephalography (EEG). After a strong initial response, the cell exhibits a weaker tonic firing component. **B, C** Time course of a minimal discharge field (MDF) of a dLGN cell and a cortical cell (area 17/V1). While the cortical cell exhibits a clear shrinkage of the MDF with progressing time after stimulation onset, the size of the dLGN field is almost constant. For the  $x, t$  plot, the data were analyzed in consecutive time windows

of 10 ms duration, and for every  $x$ -location (orthogonal to the cell's preferred orientation) the responses from all  $y$ -locations (collinear with subfield orientation) were collected. Total analysis time was identical to the time of the stimulus presentation (300 ms). **D–G** Four other examples showing cortical receptive field restructuring. The data are shown as three-dimensional plots. The shrinkage is less visible in this kind of plot but confirmed by numerical fits as described in the text

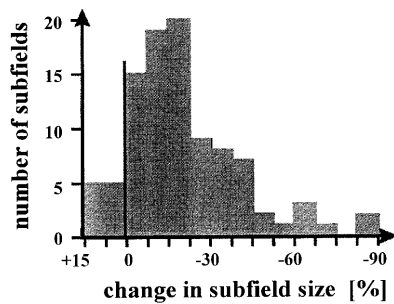


**Fig. 2** Distribution of the number of subfields versus magnitude of spatial change in subfield size over time for 107 subfield measurements in 67 cortical cells. The percentage of change  $\Delta_s$  was calculated as  $\Delta_s = \left( \frac{\text{width at 200ms}}{\text{width at 70ms}} - 1 \right) \times 100$  where time is measured relative to stimulus onset. Mean subfield shrinkage is  $22.8 \pm 12.9\%$ . Zero at the *abscissa* indicates no change in subfield size

found in cortical cells (approx.  $2^\circ$ ) and, thus, cannot explain the shrinkage of cortical RFs. Three of the dLGN relay cells (17%) showed a slight increase in RF size over time.

#### Result from the neural field model

The model we present in the following will basically explain cortical RF shrinkage by a changing *temporal* activity pattern of the afferent (dLGN) input. Along these lines we neglect the somewhat minor effect of dLGN RF shrinkage for the following two reasons: (1) the timing of the cortical RF shrinkage fits very accurately to the moment when the dLGN activity switches from phasic to tonic firing; (2) without an additional (temporal) mechanism, a reduction of 18% in dLGN RF size (which has a center size of approx.  $0.5^\circ$ ) could maximally account for an overall reduction of only 2–5% in a cortical RF (which are often  $4^\circ$  and up to  $10^\circ$  wide during the initial response) and then shrink to 1.0–3.0° during the late response). Thus, a pure spatial mechanism considering the scatter and overlap of dLGN RFs constituting a cortical subfield could account for only small changes at the margins of the cortical RFs and would not be able to result in a 22.8% shrinkage of cortical RFs during the transition from the early to the late response.

Therefore, the model was set up to test whether the afferent input from the dLGN is sufficient to produce the experimentally observed shrinkage of cortical RFs independent from dLGN RF shrinkage.

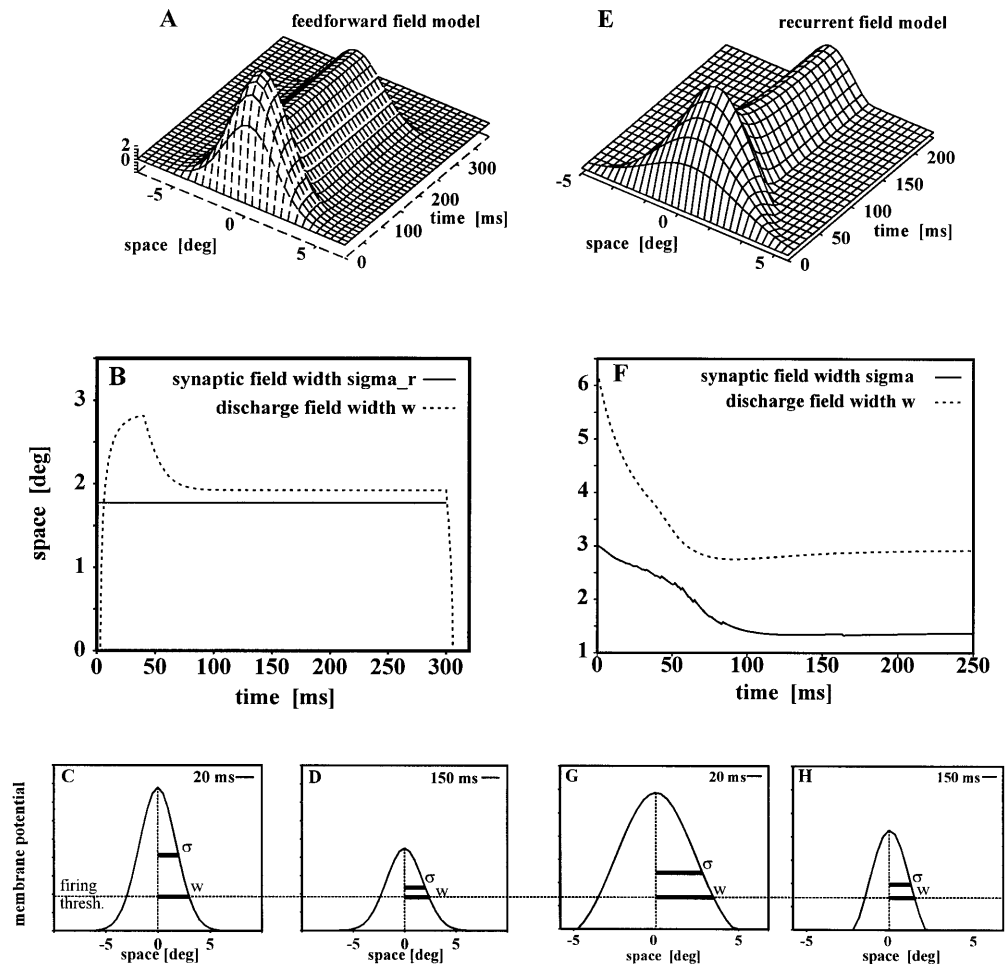
To distinguish the effect of direct afferent input from additional cortical feedback, we compared the behavior of two simple neural field models: A pure feedforward network including only the convergence of thalamocortical projections (model 1) and a network which additionally includes intracortical feedback connections (model 2). A detailed description of the neural field models is given in Appendix 1 and in more detail in (Suder et al. 2000). Here we restate only the most relevant results.

#### Cortical membrane potential and width of the discharge field

The models describe the cortical membrane potentials in space and time which result from the spatiotemporal integration of thalamic (and cortical) inputs. The phasic-tonic time course of dLGN light responses was simulated by two episodes of different firing frequency. Low-pass filtering at the thalamocortical synapse smoothes the transition from initial high to later moderate visual activity. The membrane responses can be generally simulated numerically (Fig. 3), but for the pure feedforward model they can also be calculated analytically (Appendix 1; Suder et al. 2000). Figure 3 shows simulation results for models 1 and 2. The cortical membrane potential  $V$  is plotted as a function of space and time (Fig. 3A, E). In accordance with the experimental data (see Fig. 1), a phasic peak is followed by a tonic component with a reduced amplitude. This can also be seen by looking at time slices (Fig. 3C vs D and G vs H). In both models, the suprathreshold part of the membrane potential, the MDF ( $w$ ), is wider during the initial response than during the late part of the response. By contrast, in the pure feedforward model (Fig. 3A–D), the total width of the cortical membrane potential including the subthreshold component, the D-field, has a constant standard deviation ( $\sigma_r$ ), while this parameter changes over time in the model with cortical feedback (Fig. 3E–H). Note first that the definitions of  $\sigma_r$  and  $w$  are such that, depending on the actual shape of the curves,  $\sigma_r$  can be larger (as in Fig. 3) or smaller than  $w$  (as in many of the real data sets). Changes in the width of the MDF can be attributed to an “iceberg” effect, which is a consequence of the finite firing threshold of neurons (see Fig. 8). In all model setups, we have kept the firing threshold constant over time. This was done in order to keep the model as simple as possible. Nonetheless this assumption is conservative, because, with a varying threshold, only an even stronger and faster RF shrinkage effect would be observed. In the feedforward model, the shape of the D-field is determined solely as a function of the spatial spread of the thalamocortical projections and the size of the input stimulus. In the feedback model, excitatory and inhibitory cortical inputs also shape the D-field (for details of the cortical input field, see Appendix 1). This leads also to the effect that the curves of Fig. 3B compared with F have different starting points. In the case with intracortical interactions (Fig. 3E), the first afferent activity volley triggers an intracortical interaction that results in a very wide cortical activity spread (however, with close to zero amplitude), which is not the case for pure afferent feedforward activity (Fig. 3A).

A fundamental prediction derives from the simulation results of these two models: assuming that the fit of the experimentally obtained MDFs points to a Gaussian-shaped synaptic field, the standard deviation  $\sigma$  of the D-field should systematically change over time only when intracortical feedback is involved. If, on the other hand, the temporal characteristics of the thalamocortical input

**Fig. 3A–H** Simulations of the two neural field models: *Left*: Pure feedforward; *right*: feedback model. *Top*: Simulations of the cortical membrane potential  $V(x,t)$ . *Middle*: Time courses of the receptive field width  $w$  and the standard deviation of the synaptic field  $\sigma$  for the data shown *on top*. *Left*: For the feedforward model,  $\sigma = \sigma_r$  is constant over time ( $\sigma_r = 1.772^\circ$ ; see Appendix 1), whereas  $w$  shrinks. Since the threshold is rather low,  $w$  can be larger than  $\sigma_r$ . *Right*: For the model including intracortical feedback, both measures – the standard deviation  $\sigma$  of the synaptic field (D-field)  $V(x,t)$  and the width  $w$  of the (minimal) discharge field (MDF) – show a systematic variation over time. *Bottom*: Time slices showing the spatial profile for the early burst phase (at 20 ms, corresponding to about 70 ms of real neuronal response because response latency was not implemented in the model) and the late tonic phase (at 150 ms). In both models the width of the MDF  $w$  changes over time. The standard deviation of the D-field  $\sigma$  is constant in the feedforward model (C, D) but changes significantly over time in the feedback model (G, H). Simulation parameters are given in Appendix 1



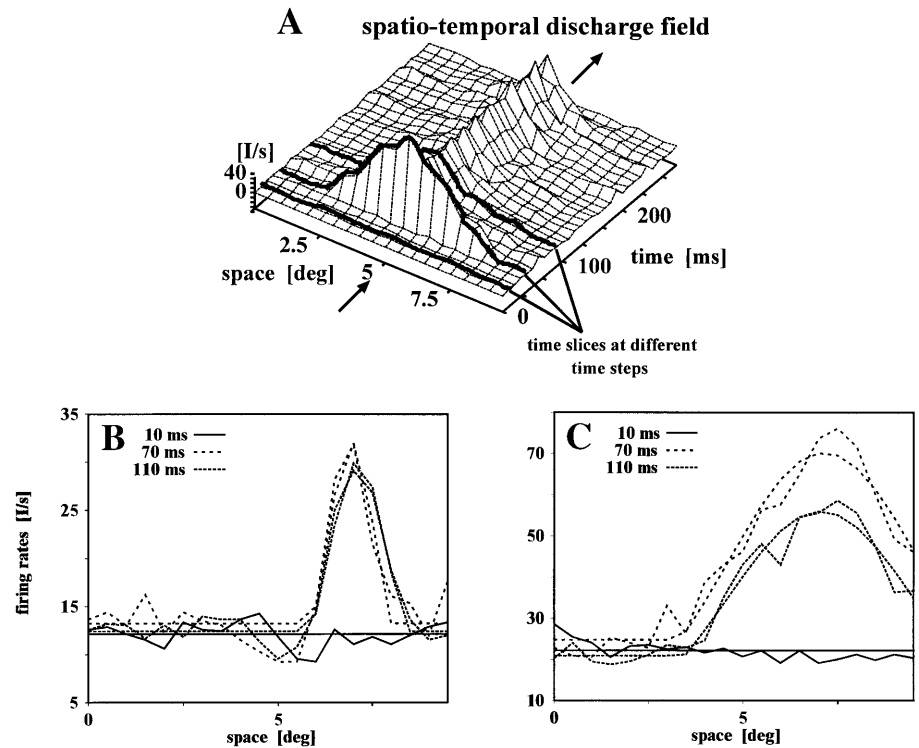
dominate the RF shrinkage effect, then the model predicts that  $\sigma$  should stay almost constant over time. This prediction is not a peculiarity of the special feedback model used here. Temporal changes in  $\sigma$  can be expected in almost all feedback models, except for the highly unlikely case that the cortical input has exactly the same spatial spread and kind of input. The anatomical data showing lateral cortical projections of different spatial range and the contribution of not only excitatory but also inhibitory inputs indicate that this case is rather unrealistic (see Wennekers 2001a, 2001b).

In a feedback model, the spatial profile of the membrane potential can be roughly envisaged as a superposition of spatial components resulting from the excitatory dLGN input and the excitatory as well as inhibitory feedback (Wennekers 2001a). The relative contribution of these components, however, changes with time, since at different times different neurons and, hence, synapses are activated. We get  $\sigma(t=0) = \sigma_r = 3^\circ$  (see Appendix 1 for parameters of the feedback model). Afterwards, as the firing activity rises in the cortical model layer, the standard deviation  $\sigma$  declines, because the excitatory recurrent connections are relatively strong and sharply tuned ( $\sigma_{\text{exc}} = 0.7^\circ$ ), while afferent input and inhibition are not ( $\sigma_r = \sigma_{\text{inh}} = 3.0^\circ$ ). This way, the intracortical amplification

leads to a gradual change from wide to sharply tuned spatial potential profiles. The parameter dependence of the time course of  $\sigma$  is complex and cannot be given in a closed form. Important is that a time dependence occurs in the same way in other feedback models for almost all parameter values if the network reveals a dynamic response that is dominated by differently tuned synaptic projections at different times. The above argumentation implies that the time-dependent change of  $\sigma$  does not necessarily have to be in the form of a shrinkage; in the model it is also possible to obtain an increasing  $\sigma(t)$  if  $\sigma_{\text{exc}}$  is considerably larger than  $\sigma_r$  and  $\sigma_{\text{inh}}$ . Anatomical results, however, indicate that a Mexican-hat profile, with  $\sigma_{\text{inh}} > \sigma_{\text{exc}}$  and relatively sharply localized excitatory couplings, is the biologically most plausible situation (Salin and Bullier 1995). In that case a shrinking  $\sigma$  of the synaptic field appears in feedback models in response to flashed stimuli.

Overall, for theoretical reasons, we conclude that a constant standard deviation  $\sigma$  of the synaptic field – as found in the feedforward model – can only be expected for very special, unrealistic, and nongeneric conditions in a feedback model. Therefore, a constant  $\sigma$  in the experimental data would be a strong indicator for a pure feedforward mechanism of the observed RF restructuring.

**Fig. 4** **A** The spatial fit. Thirty sections across the width of the receptive field (every 10 ms) are fitted. **B** Original data and fit of a cortical simple cell (on-field) to the Gaussian-shaped, analytical spatial activity profile for three selected time slices  $t_i$ . Because the response to the stimulus does not start before approximately 50 ms (response latency) in the displayed examples, the profile at 10 ms, which is best fitted by a constant value, gives an impression of the mean background activity. After the steep initial rise, the activity declines with progressing time (70–110 ms). **C** Spatial fit for another example (off-field)



#### Results of the model fitted to the data

In order to test which of the two models can explain the observed shrinkage of RFs in cat visual cortex during the situation of flashing spot stimulation, we fitted the experimental RF data to the equations given for the network activity of the neural field models (see Appendix 1; Suder et al. 2000). Details of the fitting procedure can be found in Appendix 2.

#### Fitting the spatial parameters

The fitting proceeded in two steps: first, we fitted spatial slices of the RF maps to obtain the parameters  $w(t_i)$  and  $\sigma(t_i)$  at consecutive times  $t_i$  (see thick lines in Fig. 4A; time bin is 10 ms). In a second step, the time course of the amplitude response was fitted. The goal of the spatial fitting procedure was to provide a sequence of fitted standard deviations,  $\sigma(t_i)$ ,  $i=1,2,\dots$ , which were compared with the model predictions shown in the  $\sigma$ -plots in Fig. 3. For that purpose, we tested whether  $\sigma(t)$  was constant as predicted by the feedforward model. This test would have been impossible if the whole spatiotemporal data set was fitted at once.

As an important point, we also note that through this fitting procedure it became possible to estimate the standard deviation of the subthreshold D-field  $\sigma$  from the experimentally obtained suprathreshold discharge field (MDF). In Fig. 4 spatial fits are shown for different time slices. Apparently, the experimental data can be described very well by the simple neural field model, al-

though the cells differ significantly in their spatiotemporal MDF profiles (Fig. 4A vs B).

To quantify the quality of the fit, we determined the percentage of fluctuations in the data  $[y(x)]$  which remained after subtracting the model fit  $f(x)$ , i.e., we calculated:

$$P = \frac{1}{N-1} \sum_{i=1}^N \frac{(y(x_i) - f(x_i))^2}{y(x_i)^2}, \quad (1)$$

separately, for the fit in space and in time. Averaged over all spatial fits (each of the subfields was sampled at 30 different time steps), we found  $P=0.092 \pm 0.059$ , which means that on average only 9% of the variation in the data cannot be explained by the fit.

Furthermore,  $P$  is of the same magnitude as the "noise" contained in the data. The latter can be quantified by the standard deviation of the background activity (approx. 10%) during the first 30 ms of the response, where the dLGN firing does not yet influence cortical firing. Comparability of both measures – background noise and fitting error – implies that the model consistently describes the deterministic variation in the data (Press et al. 1993).

#### Standard deviation $\sigma$ is constant over time

As outlined previously, the pure feedforward model and the model with additional feedback makes a distinct prediction concerning the temporal behavior of the standard deviation  $\sigma$  of the subthreshold depolarization field dis-

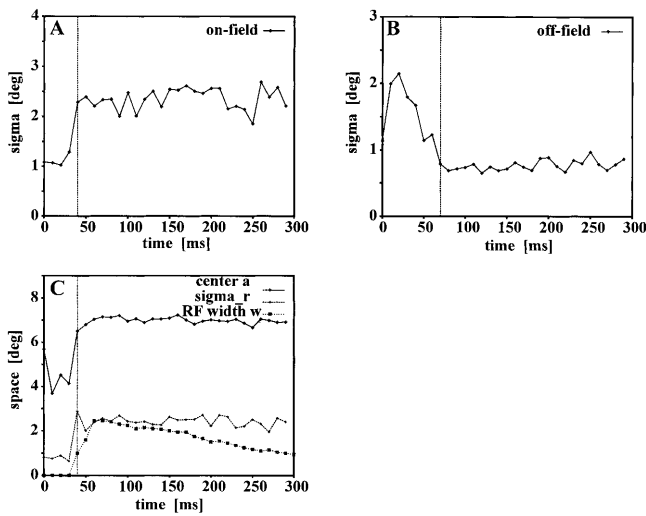


**Fig. 5A–C** Time course of the model parameters obtained from the spatial fit. Note that the dLGN activity does not reach V1 before approximately 40 ms (*left of the vertical lines*); up to that time, background noise is fitted and the resulting fit parameters are meaningless. **A, B** Time course of the standard deviation of the D-field  $\sigma$  for two example neurons. On-subfield (**A**) and off-subfield (**B**) of one neuron show both a constant  $\sigma$  over time as predicted by the feedforward model (Fig. 3B). The latency of the onset response (*vertical lines*) is larger for the off-subfield (**A** compared with **B**). **C** On-subfield of another neuron, for which, in addition to  $\sigma$ , two other parameters are plotted – offset  $a$  of the center of the fitted Gaussian (compare Appendix 1) and half-width at baseline of the extracellular MDF profile  $w$ . It can clearly be seen how  $w$  systematically changes over time, while  $\sigma$  is constant from the very beginning of thalamic input

tribution  $V$  (D-field). In the feedforward model  $\sigma$  is constant over time, whereas it varies systematically in the feedback model.

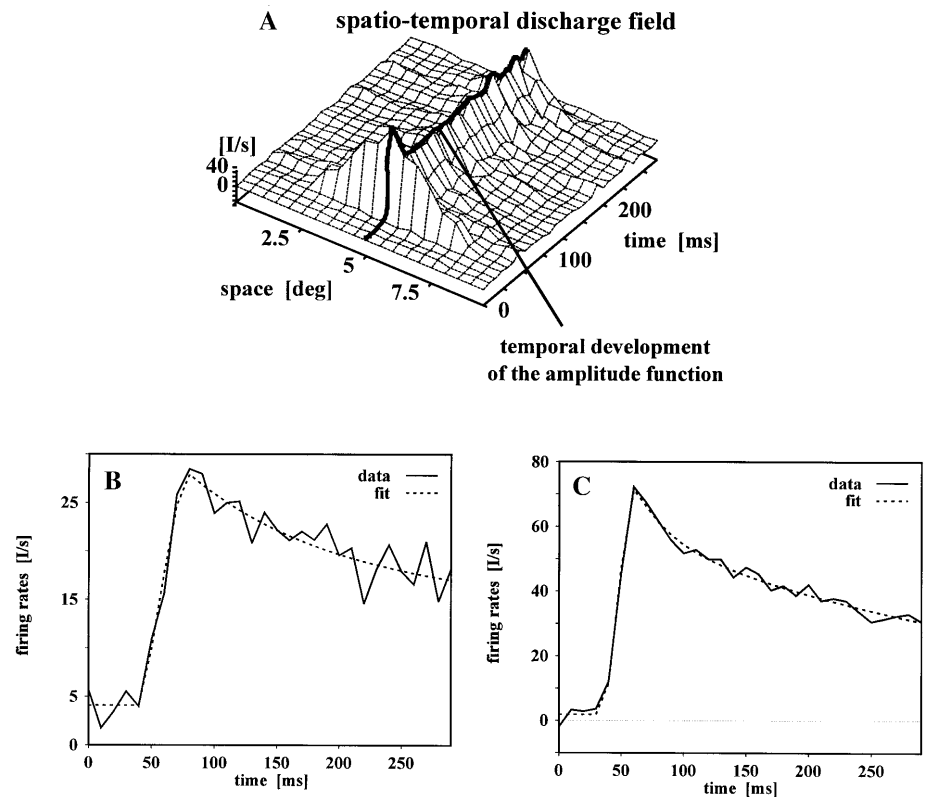
Thus, to identify the mechanism underlying the observed MDF restructuring, it is most important to examine how the fitted standard deviation  $\sigma(t_i)$  behaves over time. Figure 5A–C shows the standard deviation of the cortical D-field plotted as a function of time for three different examples of neurons. After the activity had reached V1 (approx.  $t_0=40$  ms in Fig. 5A),  $\sigma$  was constant over time. This was the case in almost all sampled subfields. Only two subfields revealed slight and insignificant trends toward larger values of  $\sigma$  with increasing time.

As a measure for the width of the MDF, we chose its half-width at baseline  $w$  (see Fig. 8). Contrary to  $\sigma$ ,  $w$  was clearly time dependent, increasing during the initial response and decreasing with the transition to the late, tonic response (see Figs. 5C, 3B). This is in accordance with the feedforward model, but not the feedback model.

#### Fitting the temporal parameters

The results of the spatial fit showed that the feedforward model describes the experimental data better than the model including feedback. Thus, we do not consider the feedback model further, but focus on the feedforward model. Additional evidence of the validity of the feedforward model will be given later by considering cortical

**Fig. 6 A** The temporal fit. **B** Original data and fit to the temporal activity  $q(t)$  of a cortical simple cell (on-field). **C** Fit for another example



firing latencies. Before doing so, we fitted – as the second step after the spatial fit – the temporal dynamics of the MDF obtained during the spatial fit procedure.

Figure 6 shows the temporal fit of the response amplitudes deriving from the first step of the fit procedure. Note that the dLGN activity did not reach V1 before  $t_0 \geq 40$  ms. Background noise was fitted during the time preceding the response and, thus, the resulting fit parameters were meaningless for  $t < t_0$ . The latencies  $t_0$  obtained from the temporal fits varied between 30 and 60 ms for different subfields. Off-subfields exhibited a longer delay than on-subfields (Schiller 1992).

For most subfields, excellent fits were obtained (see Fig. 6B, C). Averaged over all 24 fits, we found  $P = 0.107 \pm 0.144$  (see Eq. 1). Some on-subfields exhibited a significant adaptation during the tonic phase (e.g., Fig. 6C, 100–300 ms). In these cases an adaptation term was added to the tonic component in the fit function.

A comparison of the fitted parameters for on- and off-subfields of the same neuron revealed only a few systematic relations. The main difference between on- and off-subfields was a delayed response for the off-fields of approximately 20 ms ( $t_0 = 56$  ms) compared with the on-fields ( $t_0 = 35$  ms), which is in accordance with the literature (Schiller 1992).

The other model parameters did not exhibit dependencies on subfield type. Especially, the parameters of the spatial Gaussian profile, i.e., its center location  $a$ , the subfield standard deviation  $\sigma$ , and  $w$ , and the firing thresholds  $\vartheta$  were in the same range for the different subfield types. Furthermore,  $a$ ,  $\sigma$ , and  $\vartheta$  were found to be constant over time.

### Fitting cortical firing latencies

The results of the spatial fits have shown that the MDF changes can already be caused by a feedforward mechanism. To further strengthen this result we can, in addition to the MDF, analyze and fit the cortical firing latencies. The mathematics for this fitting procedure are given in Suder et al. 2000. By following Suder's procedure, we found that the cortical firing latencies  $t_{\text{lat}}$  depend *quadratically* on the distance  $x$  from the MDF center in the pure feedforward model. A correlation between firing times and distance from the MDF center has indeed been observed, but the details of its dependence are still under examination (Bringuier et al. 1999; Celebrini et al. 1993; Dinse and Krüger 1994; Ikeda and Wright 1975; Wörgötter et al. 1996).

We compared the model prediction with experimentally obtained firing latencies, describing the time from the onset of the stimulus to the first significant supra-threshold response of the recorded cell. As the latencies were not directly recorded in our experiments, cortical response onset times were obtained with the following procedure: For each location  $x$ , the time step  $t_i$  at which the firing rate first exceeds the background firing rate plus twice the standard deviation of the background fir-

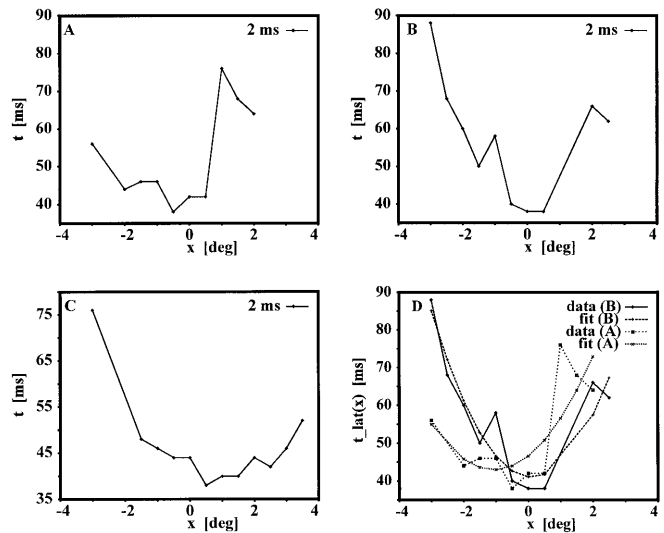


**Fig. 7A–D** Cortical firing latencies  $t_{\text{lat}}(x)$  plotted against RF location for three example fields. **A–C** Different on-subfields with 2-ms binning. **D** Quadratic fit to the data from **A** and **B**. (For clarity only two of the examples are shown)

ing was taken as  $t_{\text{lat}}$ . The binning was changed from 10 ms to 2 ms to obtain a better temporal resolution.

Because of additional noise due to the finer resolution, only 46% of all measured subfields yielded reliable estimates for the latencies and could be used for the analysis. Curves  $t_{\text{lat}}(x)$  were obtained from the experimental data and used for further analysis. In general, all curves exhibit a similar shape with longer latencies for increasing distance from the MDF center (Fig. 7). To check whether the spatial dependence can be described by a quadratic relation as predicted by the model, the data were fitted to the function  $a+bx+cx^2$  and regression coefficients were calculated. Fifty-five percent had a regression coefficient of more than 0.85. The remaining 45% of all curves exhibited regression coefficients between 0.62 and 0.74.

Assuming an intracortical axonal spread of activity, a linear dependence of the firing latencies on the distance of the MDF center was expected (Bringuier et al. 1999). Therefore, we also fitted the data with a linear model  $a+bx$ . To do so, the data were split into two halves, consisting of data points lying to the left and to the right of the shortest latency. One of the two halves was vertically mirrored and the linear fit was carried out on the resulting data including all points. Only in 18% of all cases were regression coefficients higher than 0.85. Thirty-six percent of the cells had a coefficient between 0.62 and 0.74, and for the remaining 46% it was less than 0.62.

## Discussion

Our experimental results show that the on- and off-subfields of simple (and complex) cell RFs shrank dynamically over time when the transient discharge had passed,

when stimulated with small-sized stimuli flashed for a few hundred milliseconds. An anesthetized and paralyzed preparation was used to assure stability of the eyes, which was necessary to measure this effect. Possible slow drifts of eye position cannot be entirely excluded during the long measuring period, but they would have led to an underestimation of RF shrinkage. The mean shrinkage of 23% is, thus, a conservative estimate of the effect. In addition, also the observed shrinkage in absolute terms of the RFs in the dLGN cannot account for the substantial change in cortical RF width at the transition of initial transient to subsequent tonic afferent input.

In general, these results show that the spatial characteristics of a RF also depend on the temporal structure of input activity. The activity of neurons in the primary visual cortex is, in principle, affected by mainly two input types: (1) thalamocortical inputs (feedforward projection), and (2) intracortical-corticocortical inputs (feedback projection). Both are able to shape the RF of the cortical neurons. The cortical inputs are of the feedback type, because visual activity in these circuits depends on initial input from thalamocortical afferents. This scenario is particularly relevant in a situation with little or no intracortical activity before stimulus onset. This is one of the situations which is a generic choice of stimulation in visual electrophysiological laboratories, when presenting spatially restricted and precisely timed “simple stimuli” such as flashing dots or bars. Such a protocol is used to assess the functional anatomy of the visual system, even though in a richer environment significantly more complex stimulation situations exist.

In our case, we intended to study the influence of thalamic response dynamics on cortical responses. In a previous study (Wörgötter et al. 1998), we found that during this kind of stimulation cortical RFs show changes in size depending on the state of EEG. Since thalamocortical relay cells (dLGN) show prominent, EEG-related changes in their temporal response patterns, we assumed that spatial changes of cortical RFs may be related to changes in the temporal structure of afferent input. Apart from EEG-related changes, dLGN cells also change their response from phasic to tonic *during* the time course of stimulation. Therefore, we decided to study the afferent influence on the temporal behavior of spatial characteristics of cortical RFs. To this end we needed a stimulus which optimally drives the afferent (thalamic) input to cortical cells but has a less strong driving effect on intracortical circuits. This can be achieved by a spot of light of almost the size of subcortical RFs but clearly smaller than a cortical RF subfield. A stimulus duration of 300 ms was chosen to allow development of the temporal dynamics of thalamic responses.

Another method for mapping visual RFs is the usage of patterns with randomly distributed bright and dark pixels, which are generated and changed over time by so-called m-sequences (see Reid et al. 1997). This stimulus situation is completely different from the “conventional” way of RF mapping (DeAngelis et al. 1993), be-

cause the continuously changing pattern will lead to ongoing activity in a much larger population of afferent inputs and additional ongoing activity in intracortical circuits. The emerging RF structure will thus be the result of complex and unknown spatiotemporal interactions between numerous inputs, while the conventional map shows the spatiotemporal dynamics of a single response to stimulation at a single locus. Our intention was to study the effects of thalamocortical input in isolation and therefore we used the conventional single-stimulus procedure.

The well-determined spatiotemporal characteristics of the single spot stimulus also allowed us to simulate the resulting spatiotemporal distribution of activity in a mathematical model of the visual pathway composed of either pure thalamocortical feedforward projections or additional cortical feedback connections. The model results could then be compared with the experimentally obtained RF maps to estimate the contribution of different inputs to cortical response dynamics. The latter was done by fitting the experimentally obtained RF maps with the mathematical model. Both model versions, with and without feedback, fitted the shrinkage of the MDF  $w$  very well; however, only the pure feedforward model was able to account for the unexpected finding that the synaptic field standard deviation  $\sigma$  is constant throughout the whole response. Such a behavior can be obtained with the feedback model only under rather unrealistic assumptions. Instead, the data can be fully accounted for by a dynamically changing efficiency of the feedforward thalamocortical connections related to changes in input activity.

### Spatiotemporal structure of cortical RFs

RF changes have already been analyzed. Special emphasis has been laid in the last years on fast RF restructuring effects such as those observed by Freeman and coworkers and also by several other groups (Cai et al. 1997; DeAngelis et al. 1993, 1995; Pernberg et al. 1998) who have examined intrinsic RF dynamics in dLGN and V1. These authors show that the RF structure exhibits significant spatiotemporal changes. Freeman et al. have observed that subfield sizes and subfield polarities can dynamically change over time, that is, on-subfields can exhibit off-subfield characteristics after some time following stimulation (more than 100 ms). These effects are interpreted as intrinsic neural- and network-dynamics and not as primarily stimulus-driven.

In their experiments Freeman et al. have used rather short stimulus flashes of only 50 ms duration, which approximates the response latency of cortical visual responses. Thus the changes they observe usually happen after the stimulus had already been turned off. A stimulus duration of 300 ms as used in our study allows the thalamic cells to change their firing mode (after 30–50 ms) from phasic burst firing to tonic firing. We believe that this change of the thalamic firing mode is

the reason for the shrinkage of cortical RF measured by us and is, thus, a stimulus-driven process, while RF dynamics described by Freeman et al. may relate to mechanisms intrinsic to the cortical network. Other studies indicate that the shift of on- and off-subfields that is mostly found in direction-selective cells may also relate to the characteristic of the afferent input, assuming that thalamic relay cells with different response dynamics – e.g., lagged and nonlagged cells differing by response latency – converge on a cortical cell (DeValois and Cottaris 1998; Murthy and Humphrey 1999).

Our field models allowed quantifying the size of the MDF  $w$  by fitting the data. The fitting procedure has the interesting feature that it also allows us to estimate the size of the subthreshold depolarization field ( $\sigma$ ), which can be assumed to be of an almost Gaussian shape according to intracellular data (Bringuier et al. 1999; McLean and Palmer 1994; Reid and Alonso 1995). Both measures,  $w$  and  $\sigma$ , and their relation, as obtained from the data fit, are in agreement with data from literature: RFs are consistently smaller when obtained from extracellular rates (compare, e.g., Alonso and Reid 1995). Hirsch and colleagues have mapped RFs from intracellularly recorded potentials of striate cortical simple cells (Hirsch et al. 1998). They have found fields with diameters of up to  $4^\circ$ , consistent with a mean of  $\sigma \sim 2^\circ$  from our data. Intracellular RFs of this size are also compatible with anatomical data (Antonini et al. 1998; Chapman et al. 1991; Humphrey et al. 1985). A recent study, examining the relationship between the intracellular synaptic integration field and extracellular discharge field (MDF), has also shown clearly that the subthreshold integration field covers a wider area than the output MDF (Bringuier et al. 1999). These authors claim that the wide subthreshold field is due to an intracortical spread, while we suppose mainly a feedforward spread of activity.

#### Changing effective feedforward connectivity as a mechanism for RF restructuring

Our results, in particular, demonstrate that very fast processes in the 10- to 100-ms range are probably responsible for the observed RF changes. Besides fast synaptic plasticity (Markram and Tsodyks 1996) and spike encoder adaptation (Sanchez-Vives et al. 2000), it could be the activity pattern itself which leads to the observed changes. Aertsen and coworkers (1989) had realized this when they introduced the concept of “effective connectivity” between two cells. This concept clearly takes into account that the synaptic transmission rate for any synapses at a given target is a continuously changing quantity which heavily relies on the actual state of the system.

The effective connectivity can be changed by three main mechanisms: by a varying time structure in the afferent, feedforward input signal, by feedback loops, and by the activation history, which also includes the level of unspecific, sustained activation. We will shortly explain the different effects and discuss their role in our experiments.

The observed constant  $\sigma$  of the D-field and the successful quadratic fit of the cortical firing latencies support the first hypothesis, but this effect may dominate only in the case of spatially restricted changes in visual contrast, as obtained with small, flashing stimuli. Thus, the temporal structure of the afferent input signal determines the spatial distribution of activity inside the RF and the number of neighboring neurons activated by the stimulus. For example, the high-frequency thalamic bursts of the initial response result in a strong input to V1 within a short time, leading to a high effective connectivity. This way, also weaker synapses at the periphery of the RF of a neuron may be able to elicit suprathreshold postsynaptic responses and thereby widen the MDF. At the same time, this means that not only neurons in the center of the thalamic input field, but also laterally displaced neurons receiving a weaker collateral thalamic input are depolarized to spike threshold. This effect is also fundamental to the widening of RFs during a delta wave-dominated EEG, during which thalamic relay cells generate high-frequency burst of activity in response to local changes in contrast. By contrast, the late tonic activity leads to a weaker effective connectivity, causing suprathreshold postsynaptic response only in the center of the projection line.

Feedback loops with latencies in the millisecond range have a very strong influence on the actual efficiency of connections and can also lead to fast RF dynamics. Visual cortical cells are embedded in a heavily coupled dynamic neural system and some cortical tuning effects may be hard to explain without feedback connections. Although still a topic of ongoing discussion, this has been proposed for orientation dynamics (Adorjan et al. 1999; Ben-Yishai et al. 1995; Carandini and Ringach 1997; Douglas et al. 1999; Ferster and Miller 2000; Ringach et al. 1997; Somers et al. 1995; Wenneker 2001b; Wörgötter 1999). It is reasonable to assume that the relevance of lateral intracortical interactions will grow with the complexity, spatial extent, and temporal dynamics of stimuli and may then dominate over thalamocortical influences.

Arieli and coworkers describe a third example of how the effective connectivity can change. With the help of optical imaging, they have investigated how the cortical activity is affected by its own immediate history (Tsodyks et al. 1999). The optical signals that they measured are similar to a local, 2-dimensional EEG (or rather evoked potentials, EP) recorded with a very high spatial and temporal resolution. In addition to possible feedforward and feedback influences, they found that the activity pattern of the early past has a rather strong influence on the current network responses. This result may well be expected, because it is intuitively clear that the momentary state of the membrane potential will influence the cell responses in a very direct way.

Azouz and Gray (1999) have suggested in that context that a major effect arises through the nonlinear dynamics of the fast sodium channels. Channel inactivation is prevented by steep membrane depolarizations, and

spikes are elicited fast and reliably as opposed to shallow membrane potential transients which will lead to more jitter in the spike occurrence times (Azouz and Gray 1999). Such an effect can in our case amplify the RF shrinkage effect, because the cortical membrane potential is driven hard to threshold by the thalamic burst and is bound to stay at a rather depolarized level, due to the ongoing afferent drive, which may lead to a significant fraction of inactive sodium channels.

In summary, these results support the view that the temporal structure of the thalamic input activity is a very important parameter, which needs to be taken into account in order to explain dynamic changes in cortical RFs. With our specific, restrictive stimulus situation – using a small, flashing stimulus – we were able to show the effect of temporal dynamics of thalamic activity on spatial characteristics of cortical RFs. One possible function of this mechanism may be the automatic rescaling of RFs during different stimulus situations and different states of the system (EEG). For every change in the visual scene that causes a novel situation, the high-frequency activity, paired with wider RFs and a higher number of cortical neurons involved, guarantees the detection of the change. The following shrinkage of the RFs and the number of activated neurons during tonic activity subsequently supports the finer localization and characterization of the area of interest.

**Acknowledgements** The authors acknowledge the support of the Deutsche Forschungsgemeinschaft (SFB-509) and of the HFSP. The support by and many valuable discussions with U. Eysel are gratefully acknowledged.

## Appendix 1: neural field model

Qualitative and quantitative analysis of the data with a neural field model

In order to fit the experimental data, we designed a neural field model. It is suitable not only for a qualitative, but also for a quantitative description of the experimental data (see Suder et al. 2000).

### Theoretical basis of the model

First, we study the simplest possible field model for the description of the membrane potential distribution in the primary visual cortex: a model where the activity in V1 is completely determined by the dLGN input  $I_{\text{dLGN}}(x,t)$ , i.e., a pure feedforward model. Only in the next section will we compare the dynamics of the simple model with the one of a more complex model, which includes intracortical feedback. Both models are formulated for membrane potential distributions, i.e., synaptic fields and not discharge fields. The MDF can be obtained from the synaptic field by applying an appropriate firing threshold.

In the model, the cortical state-variable is the mean membrane potential  $V(x,t)$  of a population of neurons with

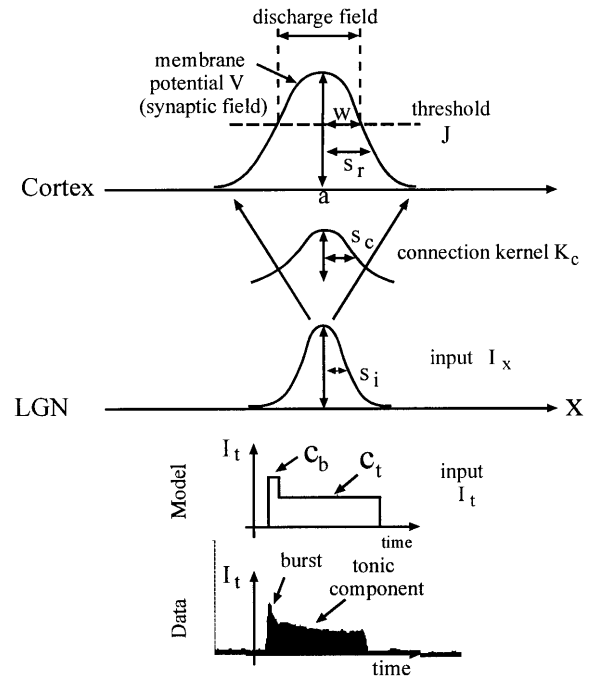


**Fig. 8** The field model and its main variables and parameters. The dLGN input is spatiotemporally separable  $[I(x,t)=I_x I_t]$ .  $I_t$  is a phenomenological model of the experimental data, reflecting the difference in firing strength and duration of burst ( $C_b$ ) versus tonic ( $C_t$ ) component (bottom). The spatial input in the form of a Gaussian with standard deviation  $\sigma_i$  ( $s_i$ ) is convolved with the Gaussian thalamocortical connection kernel  $K_c$  with  $\sigma_c$  ( $s_c$ ) leading to a Gaussian synaptic field profile  $V$ , with  $\sigma_r$  ( $s_r$ ) in V1. By thresholding the membrane potential at the threshold  $\vartheta$  ( $J$ ), the distribution of suprathreshold, i.e., firing activity, is obtained, which equals the MDF with half-width at baseline  $w$ . The temporal input  $I_t$  is low-pass filtered and leads to a modulation of the amplitude of the Gaussian profile in V1 with time. As the threshold is not changing with time, the changing amplitude will result in a changing receptive field size, which can be characterized as an “iceberg” effect. The main difference in the model with intracortical feedback is the connection kernel  $K_{\text{DOG}}$ , which is in form of a Mexican hat, mathematically modeled by difference of Gaussians

similar properties located at  $x$ . Contrary to biologically more detailed models, the neural activity  $V$  is assumed to be a function of the location  $x$  and not of discrete individual neurons, thus,  $V$  is continuous in space and time.

Just one field  $V(x,t)$  is considered, and intracortical feedback connections are first neglected but included later. For convenience, we further idealize V1 as a 1-dimensional field, i.e.,  $x \in \mathcal{R}$ , which is in accordance with our experimental data that shows no variation in the MDF dimension parallel to the preferred orientation (Wörgötter et al. 1998).

The mean membrane potential  $V$  is given by a convolution of the dLGN input  $I_{\text{dLGN}}$  and the corticothalamic connection kernel  $K_c$  (Fig. 8):

$$\tau \frac{\partial V(x,t)}{\partial t} = -V(x,t) + \int_{-\infty}^{\infty} K_c(x-x') I_{\text{dLGN}}(x',t) dx'. \quad (2)$$

Here, we include also a low-pass filter characterized by the phenomenological time constant  $\tau$  of the leakage term (Gerstner 1998).

The kernel  $K_c(x)$  describes the synaptic feedforward projection from dLGN to cortex. We choose a Gaussian connectivity profile:

$$K_c(x) = \frac{K_0}{\sqrt{2\pi}} e^{-\frac{x^2}{2\sigma_c^2}} \quad (3)$$

with effective synaptic strength  $\frac{K_0}{\sqrt{2\pi}}$  and standard deviation  $\sigma_c$ . This profile considers the fact that the connection strength decays with distance. As the anatomical connections do not change over time in our experimental setup, they are also assumed to be constant in the model.  $K_c$  represents one single on- or off-subfield. Simple cell RFs consisting of several subfields can be represented by superposition of responses of the form in Eq. 2, with appropriate kernels.

The synaptic input currents to V1 are fully described by the activity of the dLGN cells:  $I_{\text{LGN}}(x,t)$ . Thereby, detailed dynamical processes in the dLGN are not explicitly modeled but considered in the form of phenomenological, spatiotemporally separable input functions:  $I(x,t)=I_x(x)I_t(t)$ . The spatial input  $I_x$  has a Gaussian shape in our model, which represents a localized activity profile in the dLGN (Eq. 4). This corresponds to the experimental stimulus in form of a small light spot. As we did not see any changes of the spatial activity profile in the experimental dLGN data (see Fig. 1F), the assumption of a constant  $\sigma_i$  seems justified. The temporal input component  $I_t$  approximates the experimentally observed temporal firing patterns of dLGN cells (Fig. 8):

$$I_x(x) = e^{-\frac{x^2}{2\sigma_i^2}} \quad (4)$$

$$I_t(t) = c_b \Theta(t-t_0) \Theta(t_1-t) + c_t \Theta(t-t_1) \Theta(t_2-t). \quad (5)$$

The function  $I_t(t)$  describes the thalamic firing response with an initial high-frequency burst response – modeled in the form of a rectangular pulse of strength  $c_b$ , lasting from  $t=t_0$  to  $t_1$  – followed by the tonic component of height  $c_t (< c_b)$ , lasting from  $t_1$  to  $t_2$  (Fig. 8).  $\Theta(t)$  is the Heaviside function, which is zero for  $t \leq 0$  and 1 otherwise. A further assumption of the model is that the subthreshold activities in V1 are also spatiotemporally separable, i.e.,  $V(x,t)=X(x)T(t)$  (see McLean and Palmer 1989; DeAngelis et al. 1995; Mineiro and Zipser 1998). Standard simulation parameters, are  $\sigma_c=1.7^\circ$ ,  $\sigma_i=0.5^\circ$ ,  $\tau=10.0$  ms,  $t_0=0$  ms,  $t_1=40$  ms,  $t_2=300$  ms,  $c_b=80$  I/s,  $c_t=40$  I/s.

#### Neural field model with intracortical feedback

The feedforward model neglects massive corticothalamic and intracortical feedback connections, which have been suggested to cause different effects of changing receptive field dynamics (Ben-Yishai et al. 1995; Somers et al. 1995; Carandini and Ringach 1997; Adorjan et al. 1999; Bringuier et al. 1999). Therefore, it is necessary to compare the dynamics of the pure feedforward model with the dynamics of a model including also feedback connections. In separate, biologically plausible simulations, we have tested the influence of corticothalamic feedback

connections (not shown). Because these simulations demonstrated that corticothalamic feedback connections do not contribute to the observed MDF shrinkage, but rather to attentional or to other restructuring processes taking place later during the tonic phase (Wörgötter et al. 1999), we will only explore the influence of recurrent intracortical connections on the cortical potential by adding a cortical feedback loop to the simple feedforward model (Fig. 8):

$$\tau \frac{\partial V(x,t)}{\partial t} = -V(x,t) + X(x)I_t(t) + \int_{-\infty}^{\infty} K_{\text{DOG}}(x-x')R(V(x',t))dx'. \quad (6)$$

The cortical connection kernel  $K_{\text{DOG}}$  is chosen as a difference of Gaussians to include excitatory feedback for short and inhibitory feedback for long distances:

$$K_{\text{DOG}}(x) = \frac{K_{\text{exc}}}{\sqrt{2\pi}} e^{-\frac{x^2}{2\sigma_{\text{exc}}^2}} - \frac{K_{\text{inh}}}{\sqrt{2\pi}} e^{-\frac{x^2}{2\sigma_{\text{inh}}^2}}. \quad (7)$$

Parameters are such that  $K_{\text{DOG}}$  has a Mexican hat profile. The rate function  $R(V)$  in Eq. 6 is zero for  $V \leq 0$  and equal to  $\beta V$  for  $V > 0$  (see Eq. 8), where  $\beta$  is the neuronal gain (in spikes per second per millivolt). Input from dLGN is the same as in the feedforward model. Note, however, that in Eq. 6 we have already inserted the total spatial input  $X(x)$  into cortex, that is, the spatial convolution of the dLGN activity  $I_x(x)$ , Eq. 4, and the feedforward kernel from dLGN to cortex, Eq. 3. The temporal input component  $I_t$  in Eq. 6 is given by Eq. 5).

Due to the nonlinear feedback connections, analytic solutions of Eq. 6 cannot be given. Therefore, we simulate Eq. 6 and discuss the qualitative differences that appear in contrast to the simple feedforward model. As parameters, we choose  $\tau=10$  ms,  $t_0=0$  ms,  $t_1=50$  ms,  $t_2=300$  ms, and (somewhat arbitrarily)  $\sigma_i=3^\circ$ ,  $\sigma_{\text{exc}}=0.7^\circ$ ,  $\sigma_{\text{inh}}=3.0^\circ$ ,  $K_{\text{exc}}\beta=2.0$  mV/ $^\circ$ , and  $K_{\text{inh}}\beta=0.5$  mV/ $^\circ$ . Furthermore, we define  $k: k=K_0\sigma_c\sigma_i/\sigma_r$ ,  $C_1=kc_b$ ,  $C_2=kc_t$  and choose the effective cortical inputs  $C_1=10$  mV and  $C_2=2.5$  mV for the burst and the tonic phase (see Suder et al. 2000).

With these parameters the network operates in a regime of cortical amplification, as has been proposed for recurrent orientation tuning models (Ben-Yishai et al. 1995; Somers et al. 1995; Carandini and Ringach 1997; Adorjan et al. 1999). Thereby, the qualitative model behavior is comparable within a wide range of parameters (see Wenekers 2001b).

## Appendix 2: data-fitting procedure

We describe details of the fitting procedure to fit the model to the experimental data. Firing rates  $y(x,t)$  of on- and corresponding off-subfields were analyzed (see Materials and methods). Each field was sampled at 20 positions, with  $0.5^\circ$  resolution, and for 30 time slices of 10-ms bin size (or 2-ms bin size for determination of response latencies). The measurements of six off-fields

and two on-fields had to be excluded because no discharge field was detectable. In the following only the remaining subfields were analyzed.

In our extracellular recordings, firing rates and not membrane activities were recorded. The potentials  $V(x,t)$  are supposed to transform into firing rates  $R$  by means of a rectilinear function:

$$R = [\beta V - \vartheta]_+ + b, \quad (8)$$

where  $\beta$  is the neuronal gain,  $\vartheta$  the firing threshold, and  $b$  accounts for spontaneous background firing. The function  $[\beta V - \vartheta]_+$  is zero for  $\beta V - \vartheta \leq 0$  and equal to  $\beta V - \vartheta$  above zero. The feedforward neural field model described in Appendix 1 can be solved analytically, resulting in explicit formulas for the spatiotemporal profile  $V=V(x,t)$ . Those are given in Suder et al. 2000 and not repeated here. They turn out to be of the form  $V(x,t)=X(x)T(t)$ , where  $X(x)$  is a spatial Gaussian and  $T(t)$  a temporal amplitude factor. The experimentally derived firing rate data can be fitted to this analytic solution to obtain parameters of the underlying potential distribution. The fits in space give estimates of the amplitude of the response  $q$ , the center of the field  $a$ , the cortical gain  $\beta$ , the background firing rate  $b$ , as well as the synaptic field standard deviation  $\sigma$  [the standard deviation of the spatial Gaussian  $X(x)$ ], and the MDF width  $w$  defined as the half-width of the firing rate profile at baseline. All these parameters are obtained individually for 30 consecutive time slices of a response. Thus the synaptic and MDF width can be compared over time, and the amplitudes  $q=q(t_i)$ ,  $i=1\cdots 30$  can further be fitted to the temporal amplitude factor  $T(t)$  of the response expected from the analytical solution of the model. The latter fits supply firing latencies, burst durations, and stimulus offset times, although we did not discuss all these parameters in the text in detail. All fits are performed utilizing the Levenberg-Marquardt algorithm (Press et al. 1993).

## References

- Adorjan P, Levitt JB, Lund JS, Obermayer K (1999) A model for the intracortical origin of orientation preference and tuning in macaque striate cortex. *Vis Neurosci* 16:303–318
- Aertsen AMHJ, Gerstein GL, Habib MK, Palm G (1989) Dynamics of neuronal firing correlation: modulation of “effective connectivity”. *J Neurophysiol* 61:900–917
- Alonso R, Reid J-M (1995) Specificity of monosynaptic connections from thalamus to visual cortex. *Nature* 378:281–284
- Antonini A, Gillespie D, Crair M, Stryker M (1998) Morphology of single geniculocortical afferents and functional recovery of the visual cortex after reverse monocular deprivation in the kitten. *J Neurosci* 18:9896–9909
- Azouz R, Gray CM (1999) Cellular mechanisms contributing to response variability of cortical neurons in vivo. *J Neurosci* 15:2209–2223
- Ben-Yishai R, Bar-Or R, Sompolinsky H (1995) Theory of orientation tuning in visual cortex. *Proc Natl Acad Sci USA* 92:3844–3848
- Bringuer V, Chavane F, Glaeser L, Frégnac V (1999) Horizontal propagation of visual activity in the synaptic integration field of area 17 neurons. *Science* 283:695–699
- Cai D, DeAngelis GC, Freeman RD (1997) Spatiotemporal receptive field organization in the lateral geniculate nucleus of cats and kittens. *J Neurophysiol* 78:1045–1061
- Carandini M, Ringach D (1997) Predictions of a recurrent model of orientation selectivity. *Vision Res* 37:3061–3071
- Celebrini S, Thorpe S, Trotter Y, Imbert M (1993) Dynamics of orientation coding in area VI of the awake primate. *Vis Neurosci* 10:811–825
- Chapman B, Zahs K, Stryker M (1991) Relation of cortical cell orientation selectivity to alignment of receptive fields of the geniculocortical afferents that arborize within a single orientation column in ferret visual cortex. *J Neurosci* 11:1347–1358
- DeAngelis GC, Ohzawa I, Freeman RD (1993) Spatiotemporal organization of simple-cell receptive fields in the cat striate cortex. 1. General characteristics and postnatal development. *J Neurophysiol* 69:1091–1117
- DeAngelis GC, Ohzawa I, Freeman RD (1995) Receptive-field dynamics in the central visual pathway. *Trends Neurosci* 18:451–458
- DeValois RL, Cottaris NP (1998) Inputs to directionally selective simple cells in macaque striate cortex. *Proc Natl Acad Sci USA* 95:14488–14493
- Dinse HR, Krüger K (1994) The timing of processing along the visual pathway in the cat. *Neuroreport* 5:893–897
- Douglas R, Koch C, Mahowald M, Martin K (1999) The role of recurrent excitation in neocortical circuits. In: Ulinski P (ed) *Cerebral cortex*, vol 13. Kluwer Academic/Plenum, New York, pp 251–282
- Eckhorn R, Krause F, Nelson JJ (1993) The RF-cinematogram – a cross-correlation technique for mapping several visual receptive fields at once. *Biol Cybern* 69:37–55
- Eysel UT, Schweigart G (1999) Reorganization of receptive fields at the border of chronic visual cortex lesions. *Cereb Cortex* 9:101–109
- Eysel UT, Eying D, Schweigart G (1998) Repetitive optical stimulation elicits fast receptive field changes in mature visual cortex. *Neuroreport* 9:949–954
- Ferster D, Miller KD (2000) Neural mechanisms of orientation selectivity in the visual cortex. *Annu Rev Neurosci* 23:441–471
- Gerstner W (1998) Spiking neurons. In: Maass W, Bishop CM (eds) *Pulsed neural networks*. MIT Press, MA
- Gilbert CD (1996) Plasticity in visual perception and physiology. *Curr Opin Neurobiol* 6:269–274
- Hartline HK (1940) The receptive field of optic nerve fibers. *Am J Physiol* 130:690–699
- Hirsch JA, Alonso J-M, Reid RC, Martinez LM (1998) Synaptic integration in striate cortical simple cells. *J Neurosci* 18:9517–9528
- Humphrey AL, Sur M, Uhlrich DJ, Sherman SM (1985) Projection patterns of individual X- and Y-cell axons from the lateral geniculate nucleus to cortical area 17 in the cat. *J Comp Neurol* 233:159–189
- Ikeda H, Wright M (1975) Retinotopic distribution, visual latency and orientation tuning of sustained and transient cortical neurons in area 17 of the cat. *Exp Brain Res* 22:385–398
- Jones JP, Palmer LA (1987) An evaluation of the 2D Gabor filter model of simple receptive fields in cat striate cortex. *J Neurophysiol* 58:1233–1258
- Knierim JJ, Essen D van (1992) Neuronal responses to static texture patterns in area VI of the alert macaque monkey. *J Neurophysiol* 67:961–980
- Kuffler SW (1953) Discharge patterns and functional organization of mammalian retina. *J Neurophysiol* 16:37–68
- Levine MW, Shefner JM (1991) *Fundamentals of sensation and perception*, 2nd edn. Brooks/Cole, Pacific Grove, CA
- Markram H, Tsodyks M (1996) Redistribution of synaptic efficacy between neocortical pyramidal neurons. *Nature* 382:807–810
- McLean J, Palmer LA (1989) Contribution of linear spatiotemporal receptive field structure to velocity selectivity of simple cells in the cat’s striate cortex. *Vision Res* 29:675–679
- McLean J, Palmer L (1994) Organization of simple cell responses in the three-dimensional (3-D) frequency domain. *Vis Neurosci* 11:295–306

- Mineiro P, Zipser D (1998) Analysis of direction selectivity arising from recurrent cortical interactions. *Neural Comput* 10:353–371
- Murthy A, Humphrey AL (1999) Inhibitory contributions to spatiotemporal receptive field structure and direction selectivity in simple cells of cat area 17. *J Neurophysiol* 81:1212–1224
- Osaka T, Yamashita H, Kannan H (1988) A nonlinear amplifier for improving signal-to-noise ratio of single-unit recordings. *Brain Res Bull* 21:143–145
- Pernberg J, Jirrmann K-U, Eysel UT (1998) Structure and dynamics of receptive fields in the visual cortex of the cat (area 18) and the influence of GABAergic inhibition. *Eur J Neurosci* 10:3596–3606
- Press W, Teukolsky S, Vetterling W, Flannery B (eds) (1993) *Numerical recipes in C: the art of scientific computing*, 2nd edn. Cambridge University Press, Cambridge, UK
- Reid RC, Alonso J-M (1995) Specificity of monosynaptic connections from thalamus to visual cortex. *Nature* 378:281–284
- Reid RC, Victor JD, Shapley RM (1997) The use of m-sequences in the analysis of visual neurons: linear receptive field properties. *Vis Neurosci* 14:1015–1027
- Ringach DL, Hawken MJ, Shapley R (1997) Dynamics of orientation tuning in macaque primary visual cortex. *Nature* 387:281–284
- Salin P-A, Bullier J (1995) Corticocortical connections in the visual system: structure and function. *Physiol Rev* 75:107–154
- Sanchez-Vives MV, Nowak LG, McCormick DA (2000) Cellular mechanisms of long-lasting adaptation in visual cortical neurons in vitro. *J Neurosci* 20:4286–4299
- Schiller PH (1992) The on and off channels of the visual system. *Trends Neurosci* 15:86–91
- Skottun BC, Valois RLD, Groszof DH, Movshon JA, Albrecht DG, Bonds AB (1991) Classifying simple and complex cells on the basis of response modulation. *Vision Res* 31:1079–1086
- Somers DC, Nelson SB, Sur M (1995) An emergent model of orientation selectivity in cat visual cortical simple cells. *J Neurosci* 15:5465–5488
- Suder K, Wörgötter F, Wennekers T (2000) Neural field model of receptive field restructuring in primary visual cortex. *Neural Comput* 13:139–159
- Tsodyks M, Kenet T, Grinvald A, Arieli A (1999) Linking spontaneous activity of single cortical neurons and the underlying functional architecture. *Science* 286:1943–1946
- Wennekers T (2001a) Dynamic approximation of spatio-temporal receptive fields in nonlinear neural field models. *Neural Comput* (In press)
- Wennekers T (2001b) Orientation tuning properties of simple cells in area V1 derived from an approximate analysis of nonlinear neural field models. *Neural Comput* 13:1721–1747
- Wörgötter F (1999) Comparing different modeling approaches of visual cortical cell characteristics. In: Ulinski P (ed) *Cerebral cortex*, vol 13. Kluwer Academic/Plenum, New York, pp 201–249
- Wörgötter F, Eysel U (2000) Context, state and the receptive fields of striatal cortex cells. *Trends Neurosci* 23:497–503
- Wörgötter F, Opara R, Funke K, Eysel U (1996) Utilizing latency for object recognition in real and artificial neural networks. *Neuroreport* 7:741–744
- Wörgötter F, Suder K, Zhao Y, Kerscher N, Eysel U, Funke K (1998) State-dependent receptive field restructuring in the visual cortex. *Nature* 396:165–168
- Wörgötter F, Suder K, Funke K (1999) The dynamic spatio-temporal behavior of visual responses in thalamus and cortex. *Restor Neurol Neurosci* 15:137–152